Communication

Metasurfaced, Broadband, and Circularly Polarized Liquid Antennas Using a Simple Structure

Chaoyun Song, Elliot L. Bennett, Jianliang Xiao, Ahmed Alieldin, Kwai-Man Luk, and Yi Huang

***Abstract*— A novel broadband circularly polarized (CP) antenna using organic ionic liquid resonators is presented in this communication for the first time. The antenna is excited by inserting a new feeding structure into the liquid which is relatively simple but significantly improves the bandwidth and CP performance of traditional single probe-fed dielectric resonator antennas (DRAs). The proposed liquid antenna is loaded with a metasurface (MS) to further improve the impedance matching and CP characteristics. A design example of the proposed antenna shows a relatively wide fractional impedance bandwidth and CP bandwidth of 51.4% and 34.2%, respectively. In addition, the proposed liquid DRA has a reduced structural complexity and a compact size compared with the conventional DRAs with a similar performance. The design methodology presented in this communication can be further exploited for a range of new liquid DRA designs and expand the design freedom and flexibility of such antennas which may have significant implications in future antenna designs using the new liquid materials.**

***Index Terms*— Circular polarization (CP), dielectric resonator antenna (DRA), liquid antennas, metasurface (MS), organic ionic liquid.**

I. Introduction

Wideband circularly polarized (CP) antennas have been widely adopted for many wireless systems such as radio frequency identification (RFID), radar, satellite navigation, and communications [1]–[6]. Such CP antennas are capable of mitigating polarization mismatch and suppressing multipath interference, which could significantly improve the quality of communication in the aforementioned systems.

In recent years, dielectric resonator antennas (DRAs) have become increasingly popular and identified as suitable candidates for developing wideband CP antennas [7]–[12]. Traditional DRAs are typically made using solid materials (e.g., low-loss glass and ceramic). Thus, the excitation of the CP radiation for such DRAs is mainly achieved by means of cutting the dielectric resonator (DR) shapes [7], [13], [14] and/or introducing additional feeding networks [15]–[18]. As a consequence, the cost and manufacturing complexity of these conventional CP DRAs are relatively high. In addition, the solid material-based DRAs typically have limited capability to accommodate special feeding structures, especially when the antenna feed is inserted into the DRA. Therefore, these antennas generally have restricted design freedom and performance.

Manuscript received October 29, 2018; revised March 28, 2019; accepted April 6, 2019. Date of publication April 15, 2019; date of current version July 3, 2019. This work was supported by the U.K. Engineering and Physical Sciences Research Council (EPSRC) under Grant EP/P015751/1. *(Corresponding author: Yi Huang).*

C. Song, A. Alieldin, and Y. Huang are with the Department of Electrical Engineering and Electronics, University of Liverpool, Liverpool L69 3GJ, U.K. (e-mail: chaoyun.song@liv.ac.uk; yi.huang@liv.ac.uk).

E. L. Bennett and J. Xiao are with the Department of Chemistry, University of Liverpool, Liverpool L69 7ZD, U.K. (e-mail: elliot.bennett@liv.ac.uk; jxiao@liv.ac.uk).

K.-M. Luk is with the Department of Electronic Engineering, City University of Hong Kong, Hong Kong, and also with the State Key Laboratory of Terahertz and Millimeter Waves, City University of Hong Kong, Hong Kong (e-mail: eekmluk@cityu.edu.hk).

Color versions of one or more of the figures in this communication are available online at http://ieeexplore.ieee.org.

Digital Object Identifier 10.1109/TAP.2019.2911332

Liquid antennas have attracted increased research interest due to their advantages in realizing small, transparent, reconfigurable, and flexible antennas for emerging and future applications [19]. Water-based DRAs have been successfully demonstrated in laboratories with limited real-world applications [20]–[24]. The main drawbacks of water may include the relatively high dielectric loss at higher frequencies, temperature-dependent performance, and phase changes such as turning to ice if the temperature goes below 0 °C. To address these drawbacks, some dielectric solvents have been selected for use in place of water, due to their much smaller loss tangent (LT), stable dielectric relaxation, and lower freezing point [25]. However, such solvent-based liquid antennas still have problems. For example, most organic solvents are flammable and with high vapor pressures, resulting in high evaporation rates and potential safety concerns.

To overcome the aforementioned challenges, here we present a novel broadband CP antenna design using new ionic liquid materials with attractive material properties. Moreover, a novel yet simple feeding structure consisting of a single metal probe is introduced to excite a wideband CP radiation for the liquid antenna. A metasurface (MS) is utilized in the proposed design to further improve the CP characteristics and device performance. The proposed liquid antenna has shown a greatly improved wideband CP performance with much-reduced complexity compared with traditional designs. This work also offers a new idea and a new material to build liquid DRAs using an inserted feed with a simple structure.

The rest of this communication is organized as follows. A new ionic liquid is introduced in Section II. The development of the new feeding structure is presented in Section III. The addition of an MS and experimental validations are discussed in Sections IV and V. Finally, conclusions are drawn in Section VI.

II. Low-Loss Organic Ionic Liquids

As a relatively new class of liquid materials, organic ionic liquids have attracted a lot of attention over the past two decades and found many important applications, such as heat storage, liquid crystals, electrolytes, solvents, analytics, lubricants, and additives [26]. This is due to their excellent properties of thermal stability, extremely low vapor pressure, tunable electric conductivity, large electrochemical window, high heat capacity, and nonflammability. Room temperature ionic liquids (RTILs) usually consist of bulky asymmetric organic cations, with imidazolium cations being the most commercially available and most widely studied. Although salt water/sea water has been used for making antennas, it is not an ionic liquid but an aqueous electrolyte solution and thus ionic liquids, which by definition are completely comprised ions, have not been explored as antenna/RF materials.

For the first time, here we employ a low-loss organic ionic liquid for CP antenna designs. Such ionic liquids could have a much wider liquid range in terms of temperature, a significantly lower vapor pressure and very stable thermophysical material properties compared with water and some typical solvents. For example,

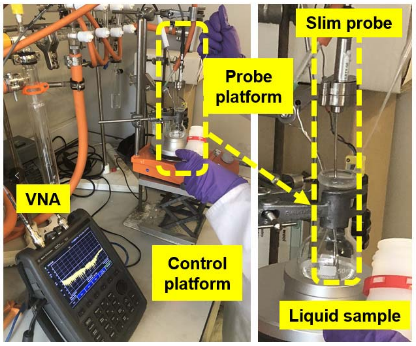

Fig. 1. Setup for the proposed organic ionic liquid measurements. A Keysight dielectric slim probe was used [30].

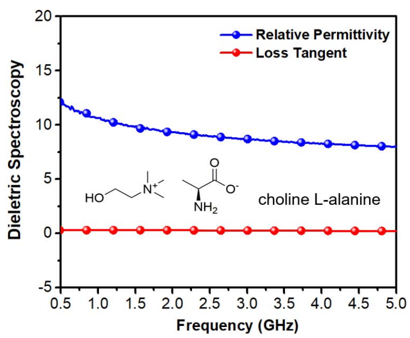

Fig. 2. Measured relative permittivity and LT of the proposed ionic liquid choline L-alanine.

an ionic liquid 1-butyl-3-methylimidazolium tetrafluoroborate (C_4MIM BF_4) has a very low freezing point down to −70 °C and an extremely high boiling point of 430 °C. However, the electrical conductivity σ of 1-butyl-3-methylimidazolium tetrafluoroborate is around 0.352 S/m, resulting in a relatively high LT for frequencies over 1 GHz. Thus, a completely organic ionic liquid (choline L-alanine) easily prepared from readily available starting materials is proposed here with a significantly lower LT. The liquid range of this compound is −56 °C–186 °C, while its electrical conductivity is as low as 0.00021 S/m [27]. Notably, such ionic liquids have no safety concerns and are typically environmental friendly. The broadband dielectric spectroscopy of choline L-alanine was measured by using a Keysight dielectric slim probe. The photograph of the measurement setup is shown in Fig. 1. The measured relative permittivity (the real part of the complex permittivity) and LT of choline L-alanine are shown in Fig. 2 over the frequency band of 0.5–5 GHz. As can be seen from Fig. 2, the relative permittivity of choline L-alanine is around 12–8 over the band, while the LT is relatively small, ranging from 0.02 to 0.1 across the band. This shows that the choline L-alanine is a suitable material for making liquid DRAs due to its low loss, low electrical conductivity, and stable thermophysical properties.

III. Novel Feeding Schemes for the Liquid Antenna

A. Traditional Single Probe Center-Fed DRA

The center-fed single probe scheme is one of the most popular feeding methods in the traditional DRA systems. An example of a cylinder liquid DRA fed by using a single straight probe is depicted in Fig. 3. The ground plane here is typically a metal sheet being electrically connected to the outer conductor of an SMA connector. The feeding probe is inserted into the liquid DR from its bottom center and is electrically connected to the inner conductor of the SMA. In this case, the $TM_{01\delta}$ mode of such cylinder DRAs could be excited [28].

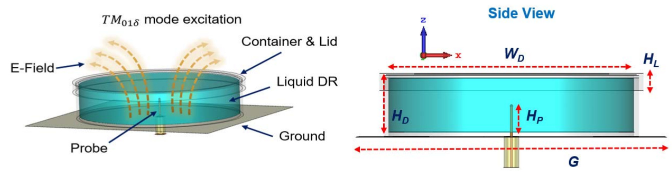

Fig. 3. Traditional single probe-fed cylinder liquid DRA and its $TM_{01\delta}$ mode. The detailed dimensions of the antenna are given in Section III-A.

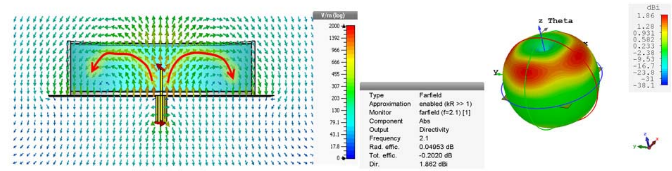

Fig. 4. Simulated (a) E-field distribution and (b) 3-D radiation pattern at 2.1 GHz of the cylinder liquid DRA using a single probe-fed scheme.

The detailed notations of the antenna parameters are shown in Fig. 3. Here, we select $W_D = 80$ mm, $H_D = 19$ mm, $H_P = 10$ mm, $H_L = 4$ mm, and $G = 100$ mm as a design example. The overall dimension of the antenna is $100 \times 100 \times 21$ mm^3. According to the design formulas of the cylinder DRA [28], the resonant frequency at the mode $TM_{01\delta}$ of this antenna using the proposed ionic liquid resonator (choline L-alanine) can be calculated using

$$k_0 r = \frac{\sqrt{3.83^2 + (\pi x/2)^2}}{\sqrt{\varepsilon_r + 2}} \quad (1)$$

$$k_0 r = \frac{f_{GHz} \cdot h_{cm} \cdot x}{4.7713} \quad (2)$$

where $x = r/h$, r is the radius of the DR ($r = 0.5 \times W_D = 40$ mm), h is the height of the DR ($h = H_D = 19$ mm), h_{cm} is the value (without units) of h in centimeters, and ε_r is the relative permittivity of the DR. As a result, the estimated resonant frequency (f_{GHz}) of $TM_{01\delta}$ mode of the proposed liquid DRA is around 2.1 GHz. Fig. 4 shows the simulated E-field distribution (2-D cut in the XOZ plane) and 3-D radiation pattern of the DRA at 2.1 GHz. It is noted that the E-field in this case is similar to that of a quarter-wavelength monopole being placed over a ground plane. The E-field is "sprayed" from the feed point and equally distributed on both sides of the probe [see arrow markers shown in Fig. 4(a)]. Such an E-field distribution leads to an omnidirectional radiation field with a maximum gain of 1.86 dBi and a radiation null at the antenna boresight direction. The simulated reflection coefficient of the aforementioned liquid DRA is shown in Fig. 5(a). It can be seen that the antenna covers a band of 2–2.2 GHz with a center frequency at 2.1 GHz, which verifies the theoretical prediction. It is concluded that the traditional single probe center-fed DRA has a limited bandwidth, low gain, and omnidirectional radiation pattern when the feeding probe is located at the bottom center.

B. Modified Feeding Scheme for the Liquid DRA

To improve the performance of the aforementioned liquid DRA, here we introduce a new feeding structure which is a combination of the traditional single probe and an extra vacant-ring structure, as shown in Fig. 6. In this scenario, the electromagnetic field distribution of the new antenna is changed. The notations of the main parameters of the vacant ring are shown in Fig. 6(b). In this example, we use $R_L = 14$ mm, $W_L = 1$ mm, and $D_L = 11$ mm. The antenna is simulated using the CST MWS software. The simulated reflection

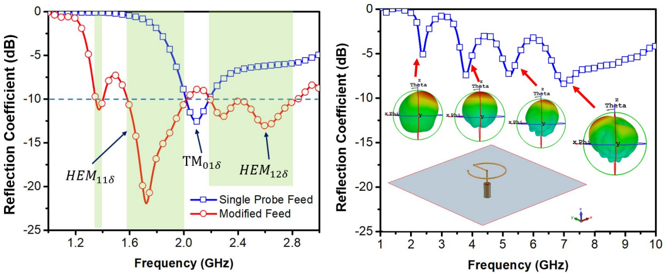

(a) (b)

Fig. 5. (a) Simulated reflection coefficients of the cylinder liquid DRA using the modified feeding scheme and the traditional single probe feed. (b) Reflection coefficient of the feed without using the liquid DR. The radiation patterns at the main resonances are given.

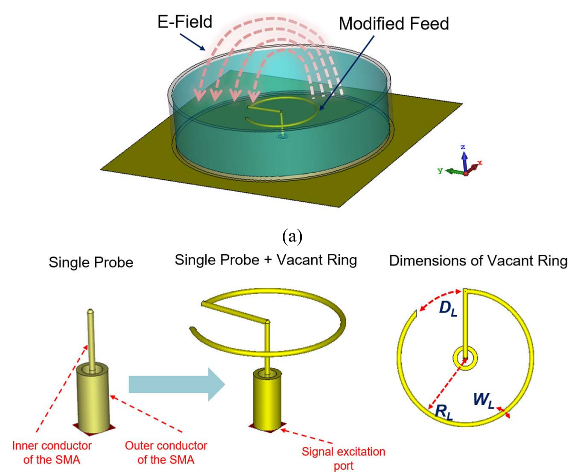

(a)

(b)

Fig. 6. (a) Proposed liquid DRA using the new feeding scheme. (The lid is hidden for a better illustration.) (b) Detailed structure and dimensions of the modified feeding structure that consists of a single probe and a vacant ring.

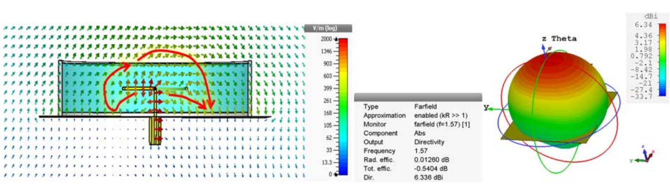

(a) (b)

Fig. 7. Simulated (a) E-field distribution and (b) 3-D radiation pattern at 1.57 GHz of the cylinder liquid DRA using the new feeding scheme.

coefficient of the proposed liquid DRA is shown in Fig. 5(a) together with that of the traditional DRA for performance comparison. It can be seen that a much wider impedance bandwidth for ($S_{11} < -10$ dB) is achieved after using this modified feed. It covers the frequency bands of 1.37–1.4, 1.6–2, and 2.2–2.8 GHz for $S_{11} < -10$ dB. The simulated E-field distribution and 3-D radiation pattern at 1.57 GHz (GPS L1 band) of the antenna are depicted in Fig. 7. It can be seen that the E-field is no longer a monopole-type distribution, as shown in Fig. 4(a). The E-field is orthogonal to the vacant ring and reflected by the ground plane in a half loop [see arrow markers shown in Fig. 7(a)], consequently forming a unidirectional radiation pattern. Such a radiation mechanism is similar to the $HEM_{11\delta}$ mode radiation of the cylinder DRA, which is hard to achieve by using a center-fed single probe scheme. The radiation pattern as shown in Fig. 7(b) is unidirectional with a greatly improved gain of 6.34 dBi.

To better understand how this new antenna works, we have first calculated the reflection coefficient of the antenna without loading the liquid. As shown in Fig. 5(b), there are four troughs around 2.4, 3.8, 5.2, and 7.5 GHz. The corresponding radiation patterns at these four frequencies are given as well. It can be seen that the antenna has a broadside radiation pattern at 3.8 GHz, while the pattern is tilted to other directions at 2.4, 5.2, and 7.5 GHz. Once the antenna is loaded with the liquid material, we can see from Fig. 5(a) that there are troughs around 1.4, 1.7, 2.3, and 2.5 GHz in its S_{11} which do not seem to be the result of simply scaling the four troughs by a factor of $\sqrt{\varepsilon_r}$ (about 3 in this case). The dielectric resonance in the antenna may have contributed to these troughs. We have then calculated the resonant frequency and quality factor (Q-factor) of the cylindrical liquid DRA under the $HEM_{11\delta}$ mode (the first mode for the excitation) using the equations as follows [28]:

$$k_0 r = \frac{6.324}{\sqrt{\varepsilon_r + 2}}\{0.27 + 0.36(x/2) - 0.02(x/2)^2\} \tag{3}$$

$$Q = 0.01007\varepsilon_r{}^{1.3} x\left\{1 + 100e^{-2.05(x/2 - x^2/80)}\right\}. \tag{4}$$

The calculated $HEM_{11\delta}$ mode resonant frequency is around 1.6 GHz and the calculated Q-factor is about 5. Therefore, the frequency bandwidth is approximately 1.6 GHz/Q = 0.32 GHz. Thus, the major trough in S_{11} between 1.6 and 2.0 GHz is due to the $HEM_{11\delta}$ mode and effect of the feeding structure. Unidirectional broadside radiation patterns are realized over the aforementioned band. We can also show that the resonant frequency for $HEM_{12\delta}$ mode is around 2.6 GHz, which is another trough observed in Fig. 5(a). Therefore, the wideband and multiband performance is likely due to the combination of the DR resonances and the wideband curl-like feed. In addition, this new feeding structure is similar to the curl antenna [31], which has realized a wideband CP radiation of the antenna.

It is worth noting that the proposed new feeding structure would be hard to realize in the conventional solid material-based DRA systems, since it would be costly and impractical to drill a special hole in solid materials (e.g., glass and ceramic) to accommodate such a vacant-ring structure. However, it is easy for the liquid DRA antenna to accommodate the proposed special feeding scheme. This is a unique advantage of the proposed liquid antenna.

IV. Metasurface Loading for Improving the Circularly Polarized Radiation

The proposed new antenna can generate a CP radiation field due to the introduction of the vacant ring. However, having conducted an in-depth optimization for the ring, we found that the frequency bandwidth for the CP radiation is limited. The state-of-the-art technology showed that the utilization of MSs could improve the CP performance for a range of typical metal/PCB antennas [29]. However, the feasibility of using the MS in DRA and liquid antenna designs has not been demonstrated before. The study here is to see if the CP characteristics of the liquid antenna could be improved by adding an MS.

The MS is normally defined as a periodic array of scattering elements with subwavelength periodicity. The structure of the MS liquid antenna is depicted in Fig. 8. It can be seen that the proposed MS consists of an array of periodic square patches and is pasted onto the lid (inner surface) of the antenna. Square patch-based MSs (SPMSs) could offer an excellent polarization independence and meanwhile generate additional resonances via the means of surface wave propagation. When the driven element underneath the SPMS is CP, the surface wave resonance could be CP as well, thus

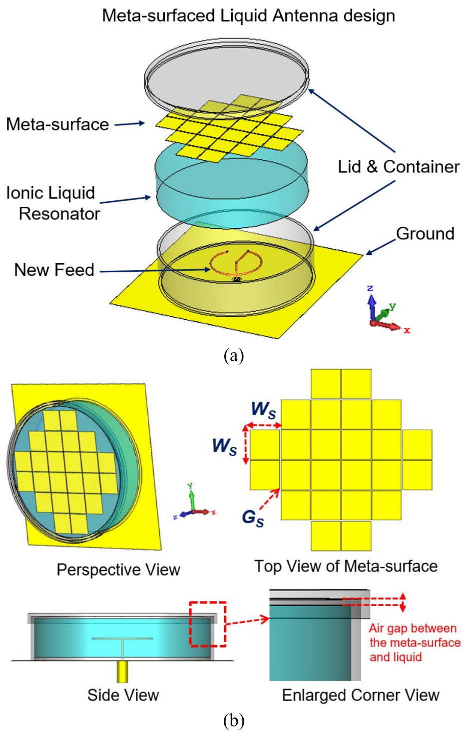

Fig. 8. Liquid DRA with an MS. (a) Disassembled view. (b) Prospective view and side view.

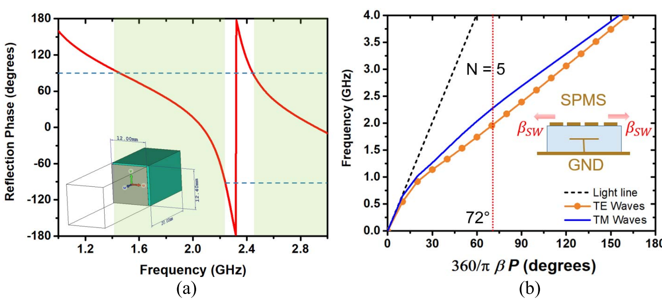

Fig. 9. (a) Simulated reflection phase diagram of the proposed MS. (b) Simulated dispersion diagram of the SPMS. The liquid resonator is modeled as the substrate.

realizing impedance and CP bandwidth improvements [29]. The unit-cell boundaries and Floquet port are employed to model the SPMS [see Fig. 9(a)]. The ionic liquid resonator is used as the dielectric substrate with a thickness of 20 mm. After optimization, the size of a single MS unit cell is $W_S \times W_S = 12 \times 12$ mm^2 with a metal patch thickness of 0.1 mm, while the gap between the cells is $G_S = 0.4$ mm. The electrical size of the unit cell at 1.57 GHz is only $0.06\lambda_0 \times 0.06\lambda_0 \times 0.0005\lambda_0$. The simulated reflection phase diagram of the proposed MS is shown in Fig. 9(a). It can be seen that the perfect magnetic conductor (PMC) bandwidth ($-90° <$ phase $< +90°$) has covered 1.4–2.2 and 2.5–3 GHz which have a good overlap with our impedance frequency bands shown in Fig. 5(a). Since the feed probe (driven element) is underneath the SPMS, the dispersion diagram of surface waves within the SPMS is also important. The frequency of the surface wave resonance can be determined by [29]

$$\beta_{SW} \times P = \pi / N \tag{5}$$

where β_{SW} is the propagation constant of the surface wave, N is the number of unit cells, and P is the periodicity of the MS. The dispersion diagram of the SPMS at the first two eigenmodes

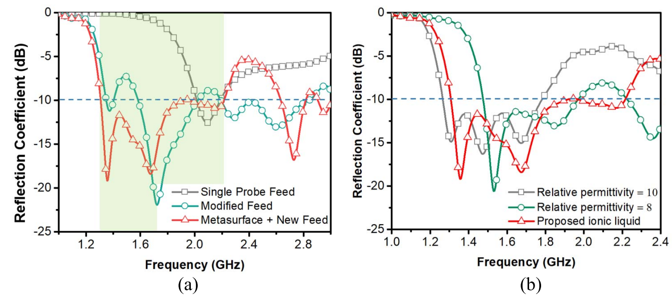

Fig. 10. (a) Simulated reflection coefficients of three-cylinder liquid DRA antennas with package. (b) Comparison between the simulated reflection coefficients of the antenna using three different materials.

[transverse magnetic (TM) and transverse electric (TE)] are simulated using the eigenmode solver of the CST and presented in Fig. 9(b). When $N = 5$, we have $360/\pi \times \beta_{SW} \times P = 72°$. The calculated resonant frequencies for the TE and TM surface waves are 2 and 2.2 GHz, respectively [see Fig 9(b)]. Since the proposed SPMS has 4×4 unit cells with 8 cell extensions (24 cells in total), the surface wave resonances of the MS are roughly at 2–2.2 GHz.

For full antenna simulation, the container and lid were modeled using Perspex acrylic with a relative permittivity of 2.5. The simulated reflection coefficient of the proposed liquid DRA with the SPMS is shown in Fig. 10(a). To make a comparison, the reflection coefficients of the previously discussed two antennas in Sections III-A (single probe feed) and III-B (modified feed) with the same package are shown as well. As can be seen from Fig. 10(a), the addition of the SPMS has improved the impedance matching between 1.3 and 1.6 GHz. The bandwidth of the MS liquid DRA for reflection coefficient < -10 dB is from 1.3 to 2.2 GHz with a corresponding fractional bandwidth (FBW) of 51.4%. However, as a comparison, the FBWs of the antennas with a single probe feed and the modified feed are just 10% and 24%, respectively. Moreover, the proposed ionic liquid material has a dielectric relaxation effect over the frequency band of interest [27]. According to Fig. 2, the relative permittivity drops from 10.5 (at 1.25 GHz) to about 8.5 (at 2.25 GHz), which have helped to improve the bandwidth of the proposed antenna. As a comparison, the simulated reflection coefficients of the proposed antennas by using dielectric materials with a fixed permittivity are depicted in Fig. 10(b). It can be seen that the resonant frequency bands for a fixed dielectric constant of 10 and 8 are about 1.26–1.8 and 1.5–2.4 GHz, respectively, in which the antenna using the ionic liquid has achieved a wider bandwidth that roughly combines the aforementioned two bands. It is worth noting that there is a tiny air gap between the MS and the liquid resonator, as shown in Fig. 8(b). The size of this air gap may slightly affect the antenna performance. It was found that the resonant frequency of the antenna goes up by increasing the size of the air gap. Therefore, in this communication, we have minimized the gap size (around 1 mm) to cover the frequency band of interest (GPS L1 band). The simulated E-field distribution and 3-D radiation pattern at 1.57 GHz of the proposed MS liquid DRA are depicted in Fig. 11. It can be seen that the E-field propagates through the MS in the antenna boresight direction. As a consequence, the antenna realizes a unidirectional radiation pattern with a maximum gain of 6.33 dBic.

To illustrate the improvement in the CP characteristics, the simulated frequency dependence of the axial ratio (AR) of the proposed antennas with/without using the MS is shown in Fig. 12. It can be seen that the minimum point of AR is shifted from 1.85 (no SPMS) to 1.6 GHz (with SPMS) after using the MS. In addition, an extra AR minimum point is observed at 2 GHz. This is due to

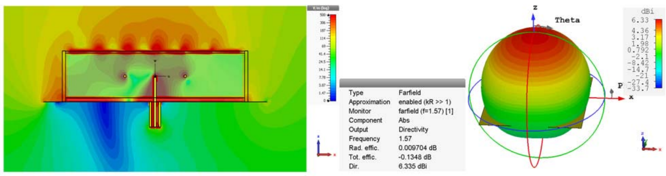
(a) (b)

Fig. 11. Simulated (a) E-field distribution and (b) 3-D radiation pattern at 1.57 GHz of the cylinder MS liquid DRA using the new feeding scheme.

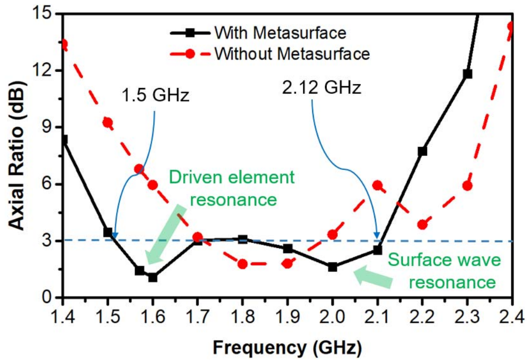

Fig. 12. Simulated frequency dependence of the AR of the proposed antennas with/without using the proposed SPMS.

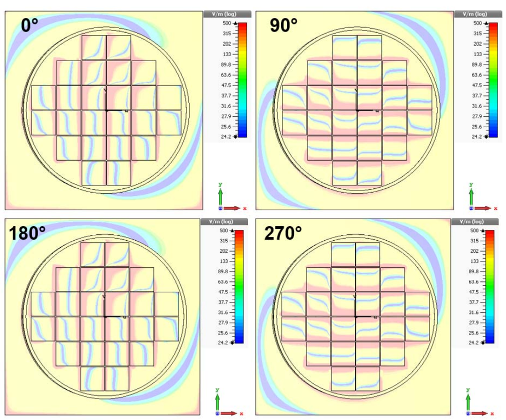

Fig. 13. Simulated E-field distributions at 1.57 GHz over the *XOZ* plane at four different phase angles.

the surface wave resonance of the SPMS as mentioned earlier. The CP bandwidth has been broadened by combining the CP resonance of the driven element (feed and DR) and the extra surface wave resonance. As a consequence, the proposed MS liquid DRA design achieves a relatively wide CP bandwidth (for AR < 3 dB) from 1.5 to 2.12 GHz (FBW $= 34.2\%$). This shows that the loading of the MS could significantly improve the CP performance of such liquid/solid DRAs. In order to gain an insightful view of the CP mechanism of the proposed antenna, the simulated E-field distributions at 1.57 GHz over the *XOY* plane are shown in Fig. 13 at four different phase angles. The E-field is rotated clockwise from 0° to 360° with a constant phase delay (90°) and a symmetrical E-field variation on the MS. This further verifies the right hand CP (RHCP) field generation of the proposed MS liquid DRA.

V. Experimental Validations and Performance Comparison

To validate the antenna performance, we have made and tested the proposed antenna prototype (see Fig. 15) based on the optimized dimensions. The cylinder-shaped container and screw-threaded

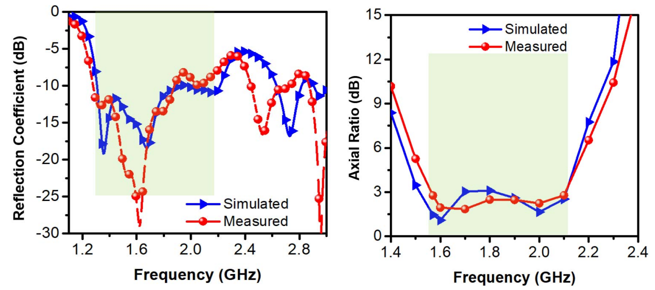

(a) (b)

Fig. 14. Simulated and measured (a) reflection coefficients and (b) ARs of the proposed antenna prototype.

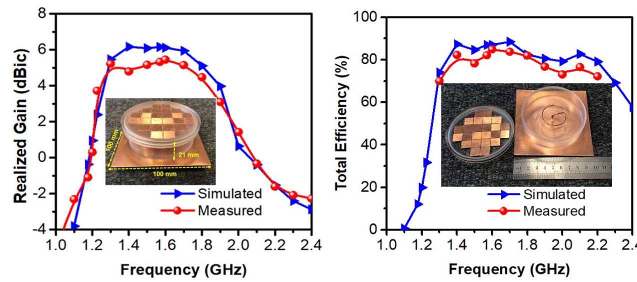

(a) (b)

Fig. 15. Simulated and measured (a) realized gains (at the antenna broadside direction) and (b) total efficiencies of the proposed antenna prototype. Photographs of the fabricated antenna prototypes are given. The overall dimension of the antenna is $100 \times 100 \times 21$ mm^3.

lid were entirely machined from a single rod of Perspex acrylic ($\varepsilon_r \sim 2.5$). The feeding probe was made using a single copper wire with a diameter of 1 mm. The antenna was measured by using a Keysight portable VNA (N9917A FieldFox). The measured reflection coefficient and AR are shown in Fig. 14 along with the simulated results for comparison.

In general, good agreement between the experimental and simulation data was obtained. The proposed liquid antenna prototype covered a band from 1.3 to 2.2 GHz, whereas its CP bandwidth (AR < 3 dB) was about 1.5–2.1 GHz. Therefore, the wideband CP performance of the antenna has been verified. In addition, it is noted that the electrical size of the antenna was reasonably compact, around $0.43\lambda_0 \times 0.43\lambda_0 \times 0.09\lambda_0$(at 1.3GHz), which was comparable to other relevant DRA designs. The simulated and measured realized gains (at the antenna broadside direction) and total efficiencies of the antenna are shown in Fig. 15. It can be seen that the antenna had a broadside radiation across 1.3–1.9 GHz, while the realized gain and efficiency were higher than 4 dBic and 80%, respectively, over the frequency band of interest. The main radiation directions at 1.9–2.2 GHz were shifted to other directions due to the higher order resonant mode generation of the DR. Thus, the realized gain at this band dropped from 5 dBic to about -2 dBic in the broadside direction. It should be noted that the introduction of the MS has improved the antenna gain by about 1 dBic over the main band of interest at 1.3–1.9 GHz. Meanwhile, the MS reduced the antenna gain by around 1.5 dBic for the band of 1.9–2.2 GHz. This was due to the increased reflection and scattering loss in this band caused by the utilization of the MS.

Moreover, the 2-D plots of the measured and simulated radiation patterns at 1.57 GHz are depicted in Fig. 16. A unidirectional radiation pattern with a relatively wide half-power beamwidth of 93° has been achieved for the RHCP radiation field. As the presented liquid antenna design example realized a wide impedance bandwidth as well as a wide CP bandwidth covering a range of GPS bands (e.g., 1.57 GHz) with a high-gain unidirectional RHCP radiation,

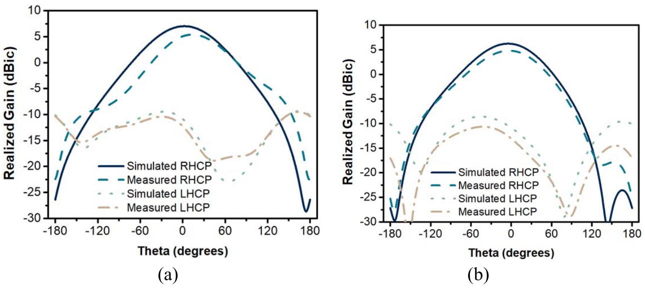

Fig. 16. Simulated and measured RHCP and LHCP radiation patterns at 1.57 GHz of the proposed antenna. (a) E-plane patterns. (b) H-plane patterns.

TABLE I
COMPARISON OF THE PROPOSED LIQUID ANTENNA AND RELATED DESIGNS

Ref. (year)	Impedance bandwidth (GHz)	CP bandwidth (GHz)	Electrical and physical size of the complete antenna
[13] (2018)	4.65 – 7.6 (FBW = 48.3%)	5.47 – 6.37 (FBW = 15.4%)	$0.78\lambda_0 \times 0.78\lambda_0 \times 0.20\lambda_0$ 50 × 50 × 12.5 mm^3
[14] (2014)	2.79 – 3.56 (FBW = 24.3%)	2.92 – 3.56 (FBW = 19.8%)	$1.3\lambda_0 \times 1.3\lambda_0 \times 0.11\lambda_0$ 150 × 150 × 11 mm^3
[7] (2018)	2.2 – 3.5 (FBW = 44.8%)	2.19 – 3.53 (FBW = 46.9%)	$0.55\lambda_0 \times 0.55\lambda_0 \times 0.14\lambda_0$ 76 × 76 × 20 mm^3
[15] (2018)	2.1 – 2.96 (FBW = 34%)	2.32 – 2.96 (FBW = 24.2%)	$0.69\lambda_0 \times 0.69\lambda_0 \times 0.27\lambda_0$ 100 × 100 × 37.5 mm^3
[25] (2018)	2.08 – 2.98 (FBW = 35.6%)	2.31 – 2.73 (FBW = 16.3%)	$0.42\lambda_0 \times 0.42\lambda_0 \times 0.23\lambda_0$ 60 × 60 × 34 mm^3
[29] (2015)	4.7 – 7.48 (FBW = 45.6%)	4.9 – 6.2 (FBW = 23.4%)	$0.5\lambda_0 \times 0.5\lambda_0 \times 0.05\lambda_0$ 32 × 32 × 3 mm^3
This work (2019)	**1.3 – 1.9* (FBW = 37.5%*)**	**1.5 – 1.9* (FBW = 23.5%*)**	$\mathbf{0.43\lambda_0 \times 0.43\lambda_0 \times 0.09\lambda_0}$ **100 × 100 × 21 mm^3**

*This represents the bandwidth for the broadside radiation with a reflection coefficient < -10 dB, AR < 3 dB and realized gain > 4 dBic at the antenna boresight.

it could be an excellent candidate for GPS and Global Navigation Satellite System (GNSS) applications.

The performance comparison between the proposed antenna and some related DRAs and some latest CP antennas are given in Table I. Our antenna achieves a relatively wide bandwidth for broadside CP radiation (with a reflection coefficient < -10 dB, AR < 3 dB, and realized gain > 4 dBic at the antenna boresight). Meanwhile, the proposed antenna has a compact size, a relatively simple structure, and fabrication process compared with the existing CP DRAs with a good performance. The height of the antenna is about $0.09\lambda_0$, which is smaller than most wideband DRA designs. The overall dimension of our antenna is comparable with that of the microstrip patch-based MS antennas [29]. Moreover, we have demonstrated the feasibility of using low-loss organic ionic liquids for such DRA designs for the first time. The new feeding scheme presented in this work has not been previously realized in the conventional solid material DRA systems.

VI. CONCLUSION

In this communication, we have presented a novel broadband CP antenna design using organic ionic liquid resonators. The liquid resonators were made of choline L-alanine with an impressive liquid range from -56 °C to 186 °C, an extremely low loss and a stable material property compared with the existing water- and solvent-based designs. In addition, a simple feeding structure formed by using a single metal probe has been designed to broaden the bandwidth, improve the gain, and excite the resonant mode of the proposed liquid antenna. The antenna has been incorporated with an MS to improve the CP performance. We have theoretically proved and experimentally verified a liquid antenna prototype that achieved a wide impedance bandwidth of 1.3–2.2 GHz as well as a CP bandwidth of 1.5–2.1 GHz. The prototype has shown a reduced structural complexity and a compact size of $0.43\lambda_0 \times 0.43\lambda_0 \times 0.09\lambda_0$ compared with prior-art designs with a similar performance. It was, therefore, suitable for a range of GNSS and communications applications. The design presented in this communication is just an example to illustrate the proposed antenna concept. The design is quite straightforward and is easy to follow. Therefore, the antenna could be easily scaled for other operating frequencies. The details of the SPMS and feeding structure could be further modified for any other specific applications. Importantly, the presented work has shown a great potential to develop novel liquid antennas using new materials and design techniques, which will attract significant research interest.

REFERENCES

[1] Y. Fan, X. Quan, Y. Pan, Y. Cui, and R. Li, "Wideband omnidirectional circularly polarized antenna based on tilted dipoles," *IEEE Trans. Antennas Propag.*, vol. 63, no. 12, pp. 5961–5966, Dec. 2015.

[2] W. Cao *et al.*, "Gain enhancement for wideband CP me-dipole antenna by loading with spiral strip in Ku-band," *IEEE Trans. Antennas Propag.*, vol. 66, no. 2, pp. 962–966, Feb. 2018.

[3] L. Zhang *et al.*, "Single-feed ultra-wideband circularly polarized antenna with enhanced front-to-back ratio," *IEEE Trans. Antennas Propag.*, vol. 64, no. 1, pp. 355–360, Jan. 2016.

[4] A. Narbudowicz, M. John, V. Sipal, X. Bao, and M. J. Ammann, "Design method for wideband circularly polarized slot antennas," *IEEE Trans. Antennas Propag.*, vol. 63, no. 10, pp. 4271–4279, Oct. 2015.

[5] D. Yu, S. X. Gong, Y. T. Wan, Y. L. Yao, Y. X. Xu, and F. W. Wang, "Wideband omnidirectional circularly polarized patch antenna based on vortex slots and shorting vias," *IEEE Trans. Antennas Propag.*, vol. 62, no. 8, pp. 3970–3977, Aug. 2014.

[6] K. X. Wang and H. Wong, "Design of a wideband circularly polarized millimeter-wave antenna with an extended hemispherical lens," *IEEE Trans. Antennas Propag.*, vol. 66, no. 8, pp. 4303–4308, Aug. 2018.

[7] M. Yang, Y. Pan, and W. Yang, "A singly fed wideband circularly polarized dielectric resonator antenna," *IEEE Antennas Wireless Propag. Lett.*, vol. 17, no. 8, pp. 1515–1518, Aug. 2018.

[8] Y.-X. Sun and K. W. Leung, "Circularly polarized substrate-integrated cylindrical dielectric resonator antenna array for 60 GHz applications," *IEEE Antennas Wireless Propag. Lett.*, vol. 17, no. 8, pp. 1401–1405, Aug. 2018.

[9] G. Varshney, S. Gotra, V. S. Pandey, and R. S. Yaduvanshi, "Inverted-sigmoid shaped multiband dielectric resonator antenna with dual-band circular polarization," *IEEE Trans. Antennas Propag.*, vol. 66, no. 4, pp. 2067–2072, Apr. 2018.

[10] B. J. Xiang, S. Y. Zheng, Y. M. Pan, and Y. X. Li, "Wideband circularly polarized dielectric resonator antenna with bandpass filtering and wide harmonics suppression response," *IEEE Trans. Antennas Propag.*, vol. 65, no. 4, pp. 2096–2101, Apr. 2017.

[11] M. Akbari, S. Gupta, M. Farahani, A. R. Sebak, and T. A. Denidni, "Gain enhancement of circularly polarized dielectric resonator antenna based on FSS superstrate for MMW applications," *IEEE Trans. Antennas Propag.*, vol. 64, no. 12, pp. 5542–5546, Dec. 2016.

[12] L. Lu, Y. Jiao, W. Liang, and H. Zhang, "A novel low-profile dual circularly polarized dielectric resonator antenna," *IEEE Trans. Antennas Propag.*, vol. 64, no. 9, pp. 4078–4083, Sep. 2016.

[13] R. Chowdhury and R. K. Chaudhary, "Investigation on different forms of circular sectored-dielectric resonator antenna for improvement in circular polarization performance," *IEEE Trans. Antennas Propag.*, vol. 66, no. 10, pp. 5596–5601, Oct. 2018.

[14] M. Zhang, B. Li, and X. Lv, "Cross-slot-coupled wide dual-band circularly polarized rectangular dielectric resonator antenna," *IEEE Antennas Wireless Propag. Lett.*, vol. 13, pp. 532–535, 2014.

[15] Y. Sun, K. W. Leung, and J. Mao, "Dual-function dielectric resonator as antenna and phase-delay-line load: Designs of compact circularly polarized/differential antennas," *IEEE Trans. Antennas Propag.*, vol. 66, no. 1, pp. 414–419, Jan. 2018.
[16] Q. Li, B. Li, and X. Wang, "A wideband circularly polarized rectangular dielectric resonator antenna with monofilar-spiral-slot fed by microstrip line," in *Proc. IEEE 5th Asia–Pacific Conf. Antennas Propag.*, Jul. 2016, pp. 103–104.
[17] L. Guo and K. W. Leung, "Compact unilateral circularly polarized dielectric resonator antenna," *IEEE Trans. Antennas Propag.*, vol. 66, no. 2, pp. 668–674, Feb. 2018.
[18] N. Yang, K. W. Leung, K. Lu, and N. Wu, "Omnidirectional circularly polarized dielectric resonator antenna with logarithmic spiral slots in the ground," *IEEE Trans. Antennas Propag.*, vol. 65, no. 2, pp. 839–844, Feb. 2017.
[19] M. Kubo *et al.*, "Stretchable microfluidic radiofrequency antennas," *Adv. Mater.*, vol. 22, no. 25, pp. 2749–2752, 2010.
[20] L. Xing, Y. Huang, Y. Shen, S. Alja'afreh, Q. Xu, and R. Alrawashdeh, "Further investigation on water antennas," *IET Microw., Antennas Propag.*, vol. 9, no. 8, pp. 735–741, Jun. 2015.
[21] L. Xing, Y. Huang, Q. Xu, and S. Alja'afreh, "A wideband hybrid water antenna with an F-shaped monopole," *IEEE Access*, vol. 3, pp. 1179–1187, Jul. 2015.
[22] C. Hua, Z. Shen, and J. Lu, "High-efficiency sea-water monopole antenna for maritime wireless communications," *IEEE Trans. Antennas Propag.*, vol. 62, no. 12, pp. 5968–5973, Dec. 2014.
[23] J. Sun and K. Luk, "A wideband low cost and optically transparent water patch antenna with omnidirectional conical beam radiation patterns," *IEEE Trans. Antennas Propag.*, vol. 65, no. 9, pp. 4478–4485, Sep. 2017.
[24] L. Xing, Y. Huang, Q. Xu, S. Alja'afreh, and T. Liu, "Complex permittivity of water-based liquids for liquid antennas," *IEEE Antennas Wireless Propag. Lett.*, vol. 15, pp. 1626–1629, 2016.
[25] Z. Chen and H. Wong, "Liquid dielectric resonator antenna with circular polarization reconfigurability," *IEEE Trans. Antennas Propag.*, vol. 66, no. 1, pp. 444–449, Jan. 2018.
[26] M. Armand, F. Endres, D. R. MacFarlane, H. Ohno, and B. Scrosati, "Ionic-liquid materials for the electrochemical challenges of the future," *Nature Mater.*, vol. 8, pp. 621–629, Jul. 2009.
[27] D.-J. Tao *et al.*, "Synthesis and thermophysical properties of biocompatible cholinium-based amino acid ionic liquids," *J. Chem. Eng. Data*, vol. 58, pp. 1542–1548, May 2013.
[28] K. M. Luk and K. W. Leung, *Dielectric Resonator Antennas*. Baldock, U.K.: Research Studies Press, 2003.
[29] S.-X. Ta and I. Park, "Low-profile broadband circularly polarized patch antenna using metasurface," *IEEE Trans. Antennas Propag.*, vol. 63, no. 12, pp. 5929–5934, Dec. 2015.
[30] *Keysight N1501A Dielectric Probe Kit 10 MHz to 50 GHz*, Tech. Overview, Santa Rosa, CA, USA, 2018.
[31] H. Nakano, S. Kirita, N. Mizobe, and J. Yamauchi, "External-excitation curl antenna," *IEEE Trans. Antennas Propag.*, vol. 59, no. 11, pp. 3969–3977, Nov. 2011.